

Laminar buffet and flow control

V. Brion, J.-C. Abart, P. Paillart

ONERA, The French Aerospace Lab

vincent.brion@onera.fr

Abstract

An experimental investigation has been conducted of the supercritical flows at transonic speeds over the laminar OALT25 airfoil in order to analyze the impact of laminar flow upon the shock wave dynamics and the existence of a laminar buffet like phenomenon. An ensemble of tests has been carried out at freestream Mach number varying in the range 0.7 to almost 0.8, angles of attack from 0.5 to 4 degrees and with different tripping configuration at the upper surface of the wing, while the boundary layer at the lower surface was forced turbulent at 7% of chord. The (airfoil) chord based Reynolds number is about 3 million. Results obtained from pressure taps and sensors measurements, as well as Schlieren visualizations of the flow, and Particle Image Velocimetry vector fields, reveal the presence of laminar buffet phenomenon in sharp contrast with its turbulent counterpart, as it features a (freestream and chord) based normalized frequency of about unity while turbulent buffet occurs for a frequency close to 0.07. While a low frequency mode, at frequency about 0.05 is also present in the laminar situation, the high frequency mode dominates the flow fluctuations. This mode exhibits strong oscillations of the shock foot and vertical deformations of the shock wave, while the low frequency peak moves the shock back and forth over a small portion of chord. The mean flow past the laminar wing is characterized by a laminar separation bubble under the shock foot, which likely contributes much to the novel dynamics revealed by the present experiments. In particular it is found that the flow instability corresponds to profound variations of the bubble extent and vortex shedding in the separated flow behind the shock wave. Two control strategies of the instability are implemented, one consisting of three-dimensional bumps and one consisting of steady jets blowing transversely to freestream. While bumps show little influence on the shock dynamics, jets successfully nullify flow unsteadiness in both laminar and turbulent conditions.

1 Introduction

Transonic buffet is one of the limitation of flight envelopes of commercial aircrafts and also limits the performance of military aircrafts engaged in air-to-air combat at high subsonic speeds due to the development of flow separation on the wing and oscillations of the shock wave which may cause the buffeting of the airframe and steep increases in drag (Ray and Taylor [26]). For civilian aircrafts certification authorities accept buffet onset boundaries based on accelerometer recordings at the pilot's seat position with peak to peak amplitudes $n = 0.25g$ (Obert [25]). From a given stable situation of the flow past an airfoil in the high subsonic regime, an increase in Mach number or angle of attack can cause the development of large oscillations of the shock wave that forms at the end of the supersonic pocket above the upper surface of the profile. This buffet phenomenon has been much described in experiments (see Jacquin et al. [15, 22, 19]) and has recently been shown to correspond to be the nonlinear saturation of a global unstable mode by Crouch et al. [9] and Sartor et al. [28]. Earlier Lee [18] proposed an acoustic feedback loop scenario to explain the buffet phenomenon, that comprises hydrodynamic waves travelling from the shock to the trailing edge, where acoustic waves are emitted that reach the shock and trigger new hydrodynamic perturbations. This mechanism was also considered by Jacquin et al. [15] and recent Particle Image Velocimetry suggest a confirmation of this scenario, see Hartmann et al. [14, 13]. Numerical simulations using RANS models and hybrid RANS-LES models have also successfully been used to simulated buffet for various airfoils [10, 3, 32, 2, 4].

Buffet onset is an important properties in the development of a wing configuration as it determines the necessary margin to critical conditions. Mabey [21] and Ray and Taylor [26] used the data of a strain gage installed at the root of an elastically similar wing to determine the oscillations of the wing structure in response to the energy provided by the shock oscillation and flow separation and obtain buffet onset. However using similarity for the wing elastic response is a difficult task and pure aerodynamical studies of the buffet, with rigid wing, is an easiest way to go. In this case criteria based on selected divergences in the static aerodynamic characteristics allow a qualitative determination of the buffet onset (see John [16]).

These previous studies concerned the shock interaction with a turbulent boundary layer, meaning, from an experimental point of view, that the boundary layer that forms at the upper surface of the wing is tripped turbulent at some location close to the leading edge. The case of an interaction with a laminar boundary layer has comparatively been much less investigated. The experimental analysis of Dor et al. [11], one of the few references in this domain, suggests the absence of marked unsteadiness in the laminar, free transition, case. Liepmann [20] stresses the importance of boundary layer effects on the shock wave phenomenon on the basis of experimental investigations of the flow past a circular airfoil. No numerical analysis seems to have been performed certainly due to the numerical and theoretical difficulty of modelling and capturing the transitional state of the boundary layer in the interaction with the shock wave. Many transition criteria exist, in a range of purely practical to stability based theoretical approaches, but no attempt of using them to describe the transitional interaction of the transonic flow past an airfoil seems to have ever been conducted. In the absence of transition criteria one has to deal with Direct Numerical Simulation (DNS) or Large Eddy Simulation (LES) which should certainly perform well to capture the situation.

The current experimental analysis aims at describing the flow behavior in the free transition case on a transonic airfoil with a laminar design. Schlichting [29] describes how the laminar flow upstream of a laminar shock wave boundary layer interaction generally separates as a consequence of the adverse pressure gradient and reattaches turbulent behind the shock wave. The laminar recirculation bubble formed in the shock foot is a strong driver for turbulence as shear instabilities (Kelvin-Helmholtz) form the initial growth for perturbations, as illustrated in the incompressible case by Jones et al. [17]. Also, Reyhner and Flugge-Lotz [27] show from numerical data that the typical fully laminar interaction creates a two stage pressure increase in the shock region, one from compression waves forming at the flow separation and that of the shock wave.

The improvement of numerical codes to capture the flow dynamics in transitional configurations relies of the availability of experimental data to confront the outputs of models or motivate their development. One key development concerns the setup of transition criteria capable of unsteady features, as this does not seem to have been developed so far. The data obtained in the current study aims at providing a reference database in this domain, with variations in Mach number, angle of attack, and considering turbulent and laminar boundary layers.

It will be shown from the experimental results that unlike the description of Dor et al. [11] an unsteady phenomenon also exists in the laminar case above critical conditions. Therefore another goal of the present study is to investigate the possibility to reduce or postpone this phenomenon. Flow control for wing operation is useful to increase flight envelope and maneuverability. Delaying buffet in the turbulent case has been established in several occasions. Cornette [8] identified a reduction in buffet intensity and a increased margin to buffet onset when using special bodies for reduced shock-induced separation, one of the basic phenomenon correlated with buffet onset. In a three-dimensional configuration Molton et al. [24] showed that mechanical, continuous, and pulsed fluidic vortex generators were capable of postponing buffet onset in a three-dimensional buffet half wing configuration, through the reduction of flow separation behind the shock wave. On this point it must be stressed that three-dimensional buffet significantly differs from two-dimensional buffet, as it implies much less shock oscillations and a wider spectral content of fluctuations.

This paper first describes the experimental setup that is deployed to investigate the flow dy-

namics in laminar conditions, taking the turbulent flow case as a preliminary validation of the experimental method and then as a reference for analysis. The second part deals with the analysis of the experimental database, that comprises mean and fluctuations of pressure at the wing surface, Schlieren visualization and visualizations based on Particle Image Velocimetry. The last section is devoted to the control of the flow using two techniques, three-dimensional bumps and steady jet blowing.

2 Description of the experiment

2.1 Wind tunnel setup

The experimental setup is an airfoil installed horizontally in the test section of the S3Ch transonic wind tunnel at the ONERA Meudon research center. The test section is 2.2m long, 0.763m in height and 0.804m in width. The Mach number in the test section can be varied from 0.3 to 1.2 and is used here in the range 0.7-0.8. Stagnation pressure in the settling chamber is equalized to atmospheric conditions ahead of the last turbulence mesh. Automatic temperature controls maintain a uniform and constant stagnation temperature of 316K. The dewpoint is controlled in order to prevent condensation in the test section.

The airfoil features the OALT25 design, an ONERA shape targetted for improved laminar flow. The airfoil is displayed in figure 2 in dimensionless units. Here the chord of the wing $c=230\text{mm}$ and the freestream velocity are considered for normalization. The Reynolds number is approximately $3 \cdot 10^6$. The angle of attack of the airfoil can be varied from 0 to 4 degrees. Note that the OALT25 design is very close to the OAT15A design which has been used in the same wind tunnel for previous tests on the buffet phenomenon (see Jacquin et al. [15]).

Adaptive upper and lower walls allow to counter test section variations due to the presence of the model and boundary layer growth at the walls so as to minimize Mach number and flow incidence changes where the wing is implemented. At first order, upper and lower walls provide contouring close to the streamlines of the flow past the wing would it be in free atmospheric conditions. Three-dimensional effects are minimized by the large aspect ratio of the wing $\lambda = \frac{s}{c} \simeq 3.5$ where s is then span equal to the wind tunnel width. Moreover there is no support inside the test section which would cause additional wakes and interactions.

An important flow parameter in the present study is the state of the boundary layer upstream of the shock wave at the suction side. In the free transition case the boundary layer remains laminar up to the shock wave. This is evidenced in figure 1 which shows the upper surface of the wing in the infrared light range with the flow coming from the left. The surface temperature shows a steep increase approximately at mid-chord as a result of the compression associated with the shock wave. An isolated roughness has been installed slightly downstream of the leading edge at a specific spanwise position to illustrate the impact of a turbulent wedge in the IR image. The wedge is easily identified in the image. By contrast, this shows that a laminar state is established in the rest of the wing up to the shock wave. In practice, IR thermography was used to check that the upper surface was free from unwanted turbulent transition. Any roughness would cause the same visualization as the one in figure 1. No IR monitoring was applied at the lower surface and thus to determine the boundary layer state it was forced turbulent by tripping tape installed at 7% of chord. The tripping tape features a sawtooth design and is taken with a thickness equal to 0.1mm when installed at 7% of chord.

To conduct IR monitoring the wing has first been painted with black mast paint of the brand Sacotherm. This increases the emissivity of the surface and improves the contrast of the IR image. Furthermore due to constraints with the optical access the IR imaging has been established through a reflection at the upper wall of the test section, which had been polished beforehand. IR thermography has been used at the beginning of the wind tunnel tests to ensure the quality of the

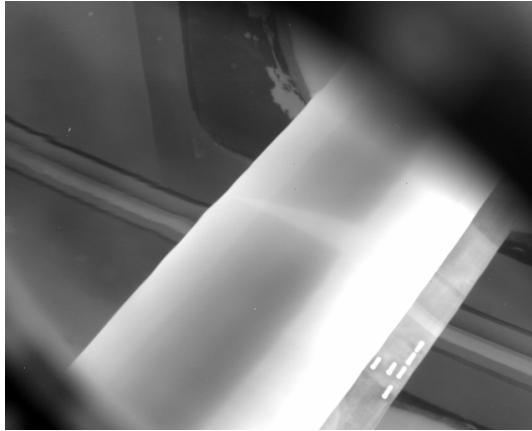


Figure 1: Infrared image of the upper surface of the wing at Mach number 0.73 and angle of attack 2 degrees. The flow comes from the left. An isolated roughness installed at the leading edge creates a turbulent wedge easily identified.

flow. In a second part of the tests an unpainted surface was used as the quality of the flow and the experience gained on the test configuration allowed to check the quality of the flow with the Schlieren visualization.

Any test is fully described by the freestream Mach number, the angle of attack of the wing and the position of the tripping that is installed at the upper surface of the wing. In the following any tests will hence be characterized by the set of parameter (M, α, tr) with M the Mach number, α the angle of attack of the wing and tr the location of the tripping tape on the upper surface in percent of chord from the leading edge. The case $tr = 0$ means free transition, i.e. no tripping tape is used. Furthermore an indication of the presence of paint (w/) or not (w/o) is given when necessary.

The first diagnostic is performed with a Schlieren visualization of the flow, on the basis of a high-speed recording (Phantom camera) at a frame rate equal to 6006fps, exposure time of $1\mu s$ and 16bits resolution per pixel. The size of the sensor is $800px \times 600px$. The intensity of the Schlieren visualisations results from an integration process of the light beams deflected by the variations in refractive index perpendicular to the knife edge that are caused by the flow [31]. For a gas refractive index is linearly related to flow density with the Gladstone-Dale constant [23]. Here the knife is set vertically and the Schlieren images show the field of $\frac{\partial \rho}{\partial x}$ that primarily highlight the shock wave and the flow structures downstream.

The wing is equipped with pressure taps and sensors, as illustrated in figure 2. Sensors and taps are aligned along two different lines which are inclined about the free stream at an angle larger than 7 degrees (the typical angle of a turbulent wedge) to prevent cross-contamination and again, early transition to turbulence. For similar reasons the fore part (20%) of the wing is free of any equipment. From 40% of chord, sensors and taps at the upper surface are almost uniformly distributed at a spacing equal to 3-4% of chord, while the lower surface has only few devices.

2.2 Validation step

The experimental setup is validated against the behavior of the flow in the fully turbulent case $tr = 7$ case, i.e. when the boundary layer at the upper surface is forced turbulent by a tripping device installed at 7% of chord. The data obtained in this configuration is compared to the one described in the work of Jacquin et al. [15] which is obtained with the supercritical OAT15A airfoil.

Figure 3 displays pressure spectra taken at the trailing edge of the wing ($x/c = 97\%$) for different

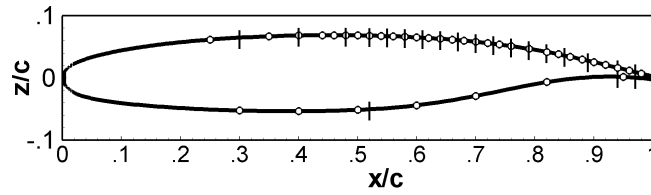


Figure 2: Pressure equipment on the wing. Circles and vertical ticks indicate pressure taps and sensors, respectively.

Mach numbers and angles of attack. The existence of critical conditions below which the flow is steady and above which it is unsteady agrees with the behavior of the flow described in Jacquin et al. [15]. Figure 3(a) illustrates the increase in fluctuation levels as α is increased and the appearance of a well marked peak when $\alpha > 3.0^\circ$ for $m = 0.75$. Similarly figure 3(b) shows that the same peak arises when the Mach number is increased above the value 0.73 for $\alpha = 4^\circ$. Both an increase in Mach and angle of attack lead to an increase in the peak level and frequency, which is about $S_t \simeq 0.07$, the same value as in Jacquin et al. [15]. These same trends were reported by Jacquin for the OAT15A airfoil, indicating that the buffet phenomenon occurs similarly on the OALT25 airfoil.

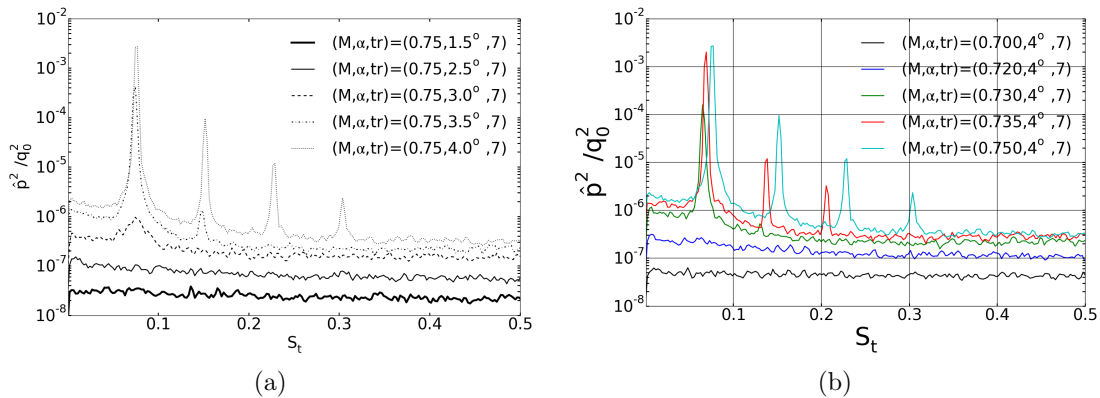


Figure 3: Pressure spectra at $x/c = 97\%$. Influence of (a) Mach number and (b) angle of attack on the shock dynamics in the turbulent $tr = 7$ case.

The flow unsteadiness is associated with a large displacement of the shock wave, as can be observed in figure 4 which shows the variation in the shock wave position. The periodic movements of the shock are synchronized with a separation of the flow downstream of the shock. Flow separation is visible from the orientation of the black area present right behind the shock wave. At the shock most upstream position, flow separation is present while at the most downstream location, the flow is attached to wing. Three-dimensional effects also appear in the course of this evolution of the flow, certainly as a consequence of flow separation which is intimately a three-dimensional phenomenon.

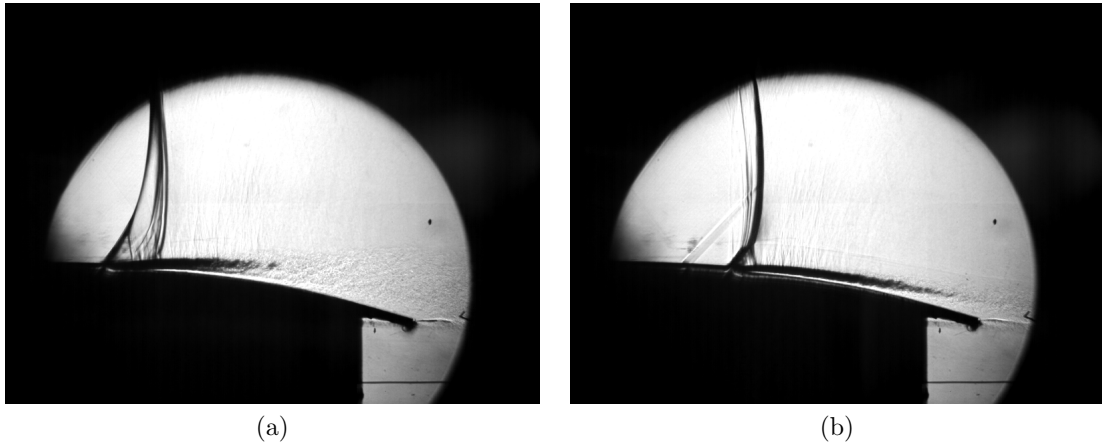


Figure 4: Schlieren visualization of the flow in the turbulent case $tr = 7$. Shock wave in (a) most upstream and (b) most downstream position.

3 Analysis and results

3.1 Exploration of the laminar dynamics

A preliminary exploration of the laminar dynamics is obtained by removing the tripping tape from the situation depicted in figure 3. Figure 5 compares the previous turbulent $tr = 7$ and the now laminar $tr = 0$ cases in terms of pressure distribution and spectra for $(M, \alpha) = (0.735, 4^\circ)$. The laminar case deviates significantly from the turbulent case. First the shock wave is located at a much more downstream location, shifting from approximately 40% of chord for $tr = 7$ to 60% of chord for $tr = 0$. The pressure plateau is also higher in the laminar case which indicates a stronger increase of the velocity at the upper surface and the extent of the shock wave is smaller which indicates weaker oscillations of the shock wave.

Pressure spectra show that the flow also exhibits an unsteadiness in the laminar case, with a dominant peak at a normalized frequency $S_t \simeq 1$ which is to be compared to the value $S_t \simeq 0.07$ in the turbulent case. Two harmonics of the main frequency peak are similarly observed in the two configurations and the primary peak levels are approximately equal. In addition to the main peak, a low frequency bump is also apparent in the laminar case at about $S_t = 0.05$.

Schlieren visualizations of the upper part of the flow are shown in figure 6. These are obtained by taking, at any pixel, the minimum intensity value over the entire duration of the record. The turbulent case demonstrates the significant chordwise oscillations of the shock wave. In comparison, the laminar case exhibits only small variations of the position of the shock. The two cases further exhibit oscillations of the flow downstream of the shock foot.

A Fourier analysis of the Schlieren images $I(x, z, t)$ in the laminar $tr = 0$ case reveals the same two dominant unsteady modes that were captured by the pressure spectra. Figure 7 shows the spectrum of $\hat{I}(x_0, y_0, S_t)$ at a location (x_0, y_0) close to the shock foot and the Fourier modes $\hat{I}(x, y, S_t)$ of the two dominant modes, at $S_t = 0.05$ and $S_t = 1$. The low frequency mode shown in figure 7(a) is distributed along the shock wave and captures its low frequency oscillations in the chordwise direction. The oscillations of the shock induced by this mode can be observed in the Schlieren record. The high frequency mode in figure 7(b) shows that the dominant mode affects the bottom part of the shock wave, and features an upward travelling wave along the shock.

Overall this preliminary comparison of the turbulent and laminar dynamics establishes that laminarity strongly affects the aerodynamics of the airfoil, in terms of forces as is apparent from

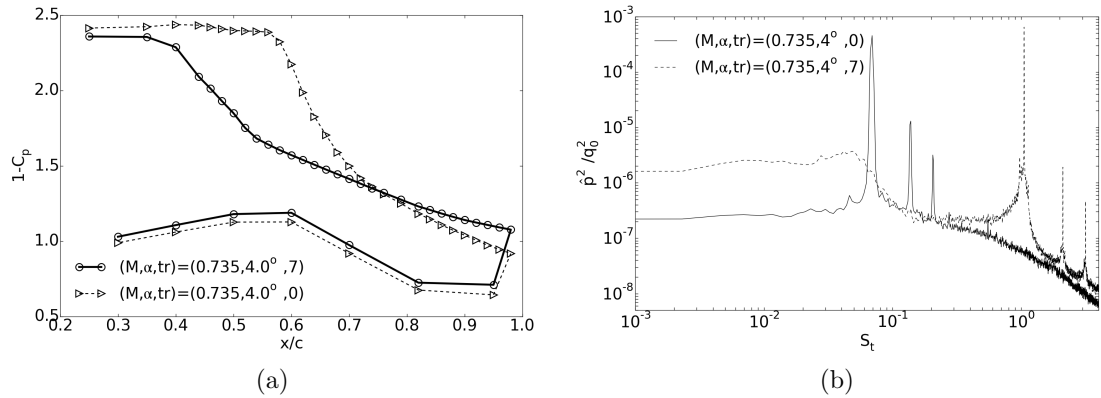


Figure 5: Minimum intensity image of the Schlieren view of the upper part of the flow. (a) turbulent $tr = 7$ and (b) laminar $tr = 0$ cases.

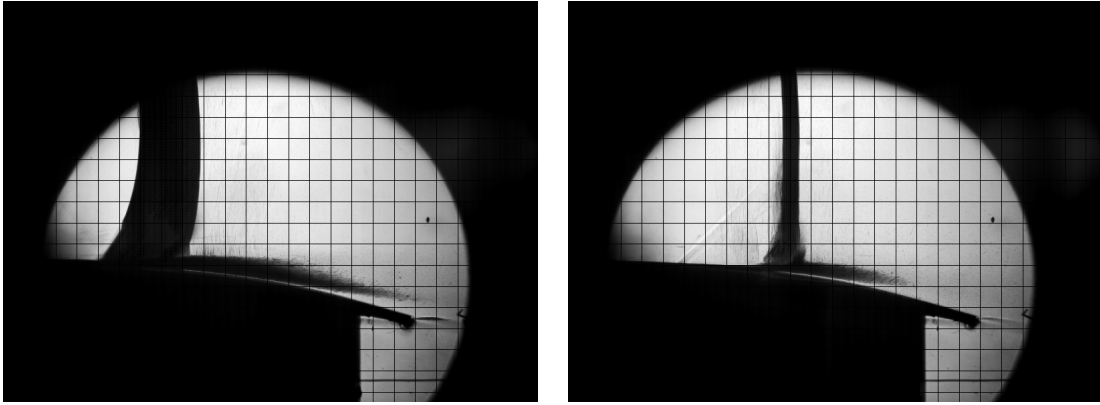


Figure 6: Comparison between the turbulent $tr = 7$ and laminar $tr = 0$ cases in terms of (a) mean C_p distribution and (b) pressure spectra at $x/c = 97\%$.

the difference in pressure distributions and in terms of flow dynamics as the laminar case introduces a reduced low frequency mode and a dominant high frequency mode that was not present in the turbulent case. This shift in the dynamics is associated with a much smaller extension of the shock movement in the chordwise direction and an intense dynamics of the shock foot. The dominant modes of the laminar setting at $M = 0.735$ are at $S_t = 0.05$ and $S_t = 1$, which must be compared to the turbulent $tr = 7$ case which features $S_t = 0.07$. The low frequency dynamics of the laminar case looks like that of the turbulent case, although the shock movement is much weaker.

3.2 Effect of Mach number and angle of attack

In this section the main features of the laminar flow are presented. Figure 8 shows the effect of angle of attack and Mach number on the evolution of pressure along the airfoil in the laminar $tr = 0$ case. In figure 8(a) the angle of attack is varied from 1.5° to 4° at $M = 0.735$. As α increases the flow at the suction accelerates more and the shock wave strengthens and is pushed downstream. In fact only a weak variation of the shock location is observed above $\alpha = 2.5^\circ$, with the maximum value being about 60% of chord. The region ahead of the shock exhibits a plateau which corresponds

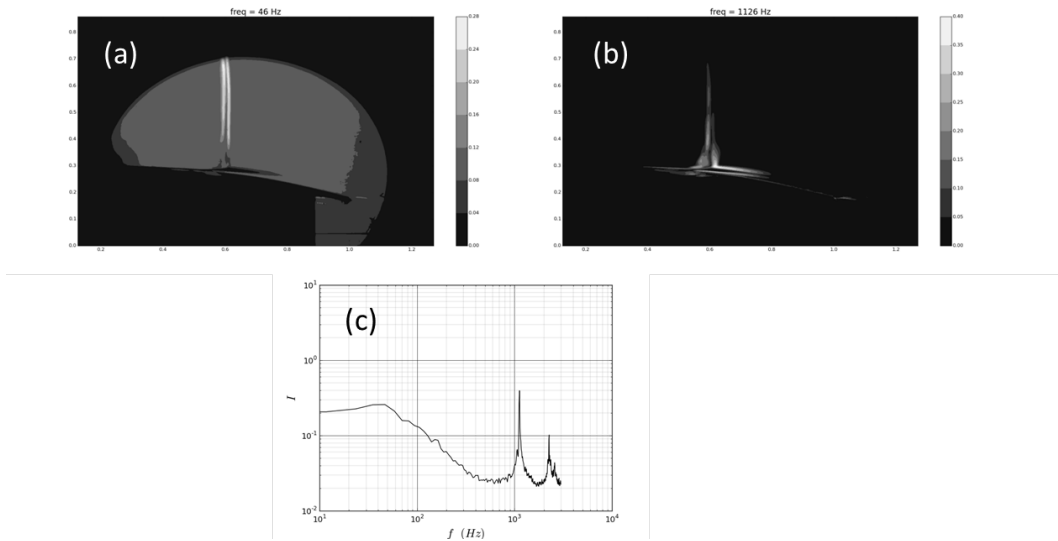


Figure 7: Spectral component analysis of the recording of the Schlieren visualization showing in (a) the Fourier mode at $S_t = 0.05$ in (b) the Fourier mode at $S_t = 1$ and in (c) the spectrum in one particular location of the Schlieren movie in the shock foot region.

to the rather geometrically flat top of the first half of the suction surface (see figure 2). Above $\alpha = 3.5^\circ$ the shock starts to spread in the streamwise direction and flow separation is apparent at the trailing edge as the mean C_p moves away from the value at lower incidences.

The increase in Mach number evaluated by figure 8(b), for $\alpha = 4^\circ$, shows that as M rises the shock is moved downstream but weakly strengthened. The shock position locks at the 60% position reported previously above $M = 0.73$ and starts to spread as the Mach is further increased. For this incidence of 4° the increase in Mach number causes a lower plateau level ahead of the shock which indicates that lift is being reduced. This agrees with the flow separation that is evidenced by the sharp increase in C_p level at the trailing edge for the highest Mach number value.

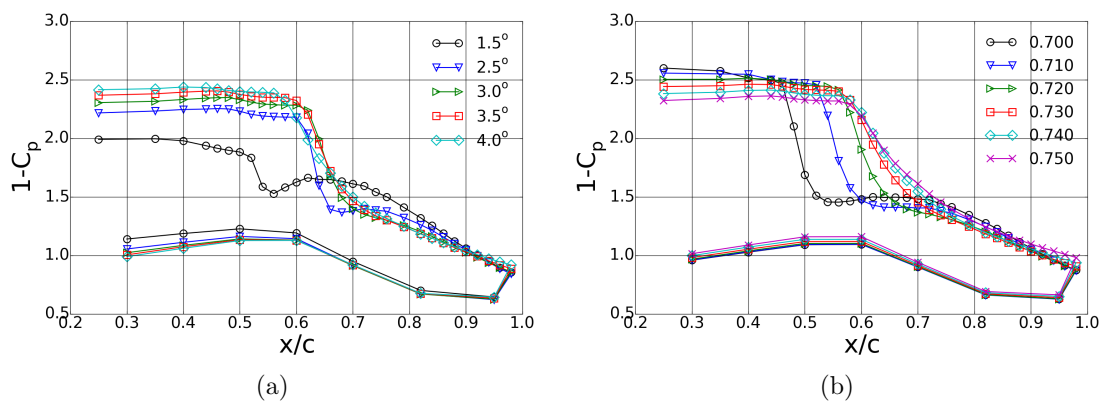


Figure 8: Effect of (a) angle of attack for $M = 0.735$ and (b) Mach number for $\alpha = 4^\circ$ on the mean pressure distribution in the laminar $tr = 0$ case.

The effect of Mach number and angle of attack on the shock dynamics is illustrated in the

pressure spectra in figure 9 with the pressure delivered by the sensor located at $x/c = 97\%$. An increase in M and α leads to a reduction of the frequency of the high frequency mode. This is opposite to the turbulent case indicating that a different flow physics is at stake here.

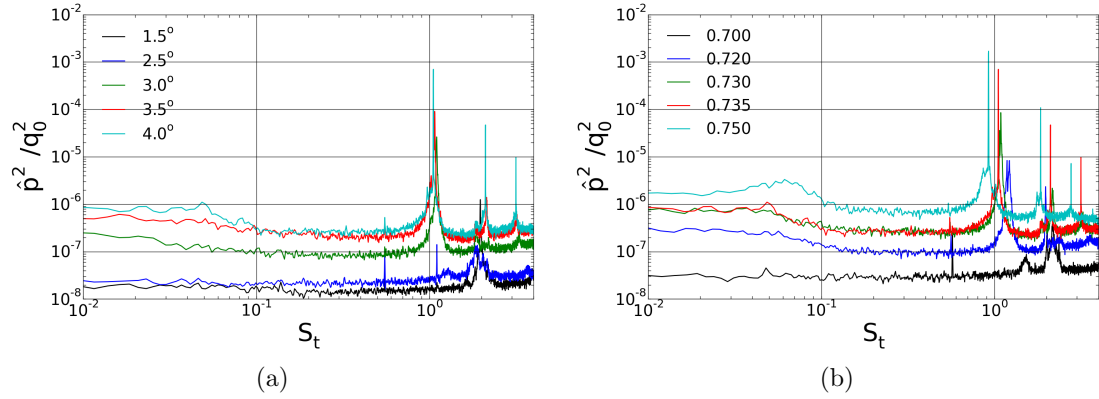


Figure 9: Effect of (a) angle of attack for $M = 0.735$ and (b) Mach number for $\alpha = 4^\circ$ on the pressure spectra for the sensor located at $x/c = 97\%$.

In figure 9(b) the low frequency peak can be observed for $M = 0.75$. Figure 10 shows more specifically the evolution of this low frequency peak as a function of angle of attack and Mach number. The low frequency peak is seen to increase in amplitude and frequency as either M or α is increased. Were it the same dynamical component as the turbulent buffet phenomenon, this evolution in frequency would match this characteristics of the turbulent buffet phenomenon described by Jacquin et al. [15]. An interesting fact that can be identified from figure 9(b) and figure 10 is that the low frequency peak seems to arise at larger values of α and M than the high frequency mode.

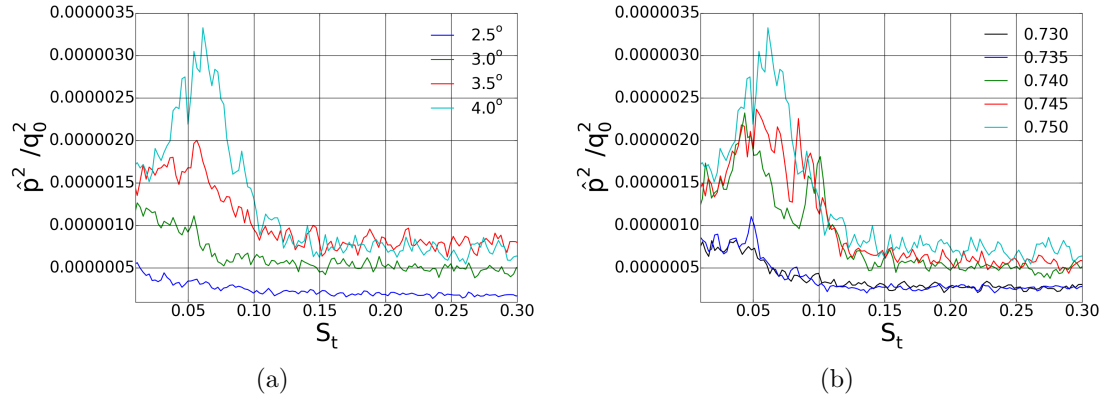


Figure 10: Zoom in the low frequency domain of the effect of (a) angle of attack at $M = 0.75$ and (b) Mach number at $\alpha = 4^\circ$ on the pressure spectra for the sensor located at $x/c = 97\%$.

3.3 Laminar separation bubble

Figure 11 shows the evolution of the variation of the mean pressure coefficient about the value C_{p0} at $x/c = 30\%$ along the suction surface with the x coordinate offset with respect to the location of the

shock wave, which is here defined as the location of maximum pressure variation in the streamwise direction. The data is shown for the turbulent $tr = 7$ and laminar $tr = 0$ cases and highlights two important features of the laminar case. The first one is the presence of a pressure rise ahead of the shock wave in the laminar case which is absent in the turbulent case and corresponds to the laminar separation of the flow, as described by Schlichting [30]. This pressure rise is followed by a pressure plateau prior to the strong compression imposed by the shock. This behavior is typical of a separation in a supersonic flow. The behavior of the flow in such a circumstance is described by the free interaction theory by means of empirical correlation, see for instance Babinsky and Harvey [1]. Laminar separation is present for all the Mach numbers illustrated in figure 11(b).

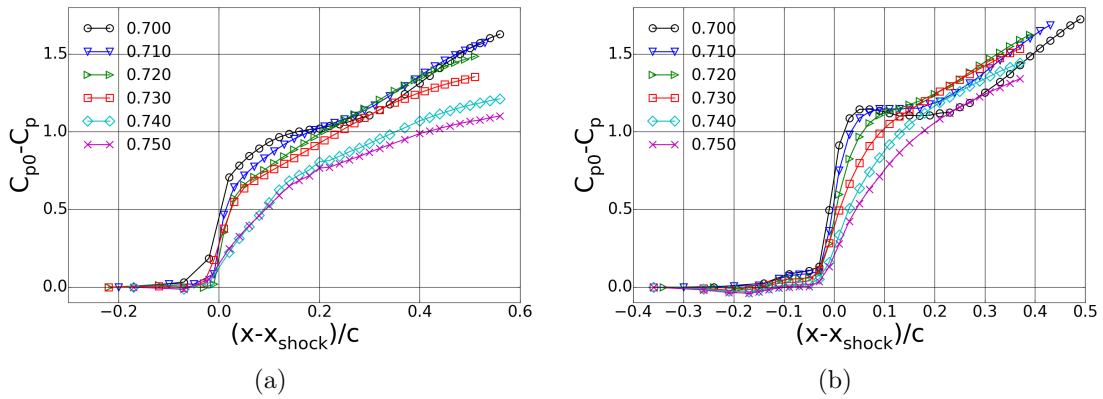


Figure 11: Effect of Mach on pressure distribution at the suction surface for the (a) turbulent and (b) laminar case. The x coordinates is referenced to the position of the shock, taken here as the location of maximum variation in pressure. The pressure is expressed as the variation of the pressure coefficient about the value C_{p0} taken at $x/c = 30\%$.

A close-up view of the region where pressure starts to rise is displayed in figure 12. In this figure, pressure is normalized on the minimum pressure p_{min} that occurs ahead of the shock wave and not on free stream properties like in figure 11(b) while axial distance remains referenced about the shock location. According to the free interaction theory the level of pressure in the plateau region $p_{plateau}$ increases with the skin friction coefficient at the separation and decreases with the Mach number outside the boundary layer. Here figure 12 shows that the pressure level decreases as the upstream Mach number increases. In the transonic regime the skin friction mainly depends on flow velocity and from figure 8(b) one can see that for $\alpha = 4^\circ$ the Mach number in the plateau ahead of the shock decreases with freestream Mach number, indicating that the skin friction also decreases. According to the free interaction theory, one should thus expect the decrease in plateau pressure that is observed.

The second feature to be observed in figure 11 is that the pressure increase due to the shock is larger in the laminar than in the turbulent case. This is to be related to the more downstream location of the shock in the laminar case, as seen in figure 5. An important consequence of the increase shock strength in the laminar case is that it should lead to higher wave drag and thus penalize the benefit of a laminar stream.

Particle Image Velocimetry (PIV) has been developed to measure the flow passing above the airfoil. In the present document only qualitative visualizations from these PIV experiments are considered, that allow to see the laminar separation and its development. Figure 13 shows the flow close to the wing suction side in the laminar separation region and materializes the frontier of the separation with natural seeding provoked by the condensation of the humidity of the air in the tunnel. Thus in this occasion no humidity control is applied. In fact this natural seeding was found

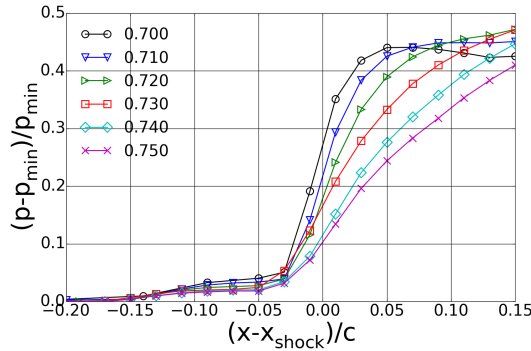


Figure 12: Same as figure 11(b)

to be a good method to visualize the flow close to the wall, which however is difficult to capture due to the small height of the separation (on the order of 1mm) and to light reflections that occur at the wall. The surface of the wing plays the role of a mirror as it is not painted and the bottom part of the image is simply the symmetric part of the top part. This symmetry allows to easily identify the location of the suction surface of the wing.

What is observed in figure 13 is a sequence of uncorrelated images (sampling rate is 4Hz) that show the separation of the boundary layer at the left, the development of the separated flow, with the recirculating flow below and the external flow above, and the development of turbulence through the action of the Kelvin-Helmholtz (KH) instability. In particular the eddies formed by the instability of the shear layer at the top of the recirculation region can be identified in these images. This sequence suggests that one of the mechanism of the high frequency peak may be the destabilization of the laminar separation bubble.

3.4 Effect of surface roughness

Surface roughness has been sampled at several locations on the wing upper and lower surfaces with and without paint. The surface roughness measuring instrument is a Mitutoyo SurfTest SJ-301 that scans over a length of 4mm at a speed of 0.5mm/s and delivers as roughness parameters the arithmetical mean Ra , the root mean square Rq and the average distance between highest peaks and lowest valleys Rz according to the Japanese Industrial Standard JIS2001. Table 1 indicates the results averaged over the ensemble of sampling locations for the different roughness situations. In particular the case with paint comprises a preliminary raw configuration that was observed to generate an early transition of the boundary layer and was then sandpapered to reduce roughness and successfully allow the laminar state up to the shock wave. The table indicates that a too high surface roughness leads to the transition of the boundary layer upstream of the shock wave. The investigation does not allow to differentiate the effects of mean and maximum roughness but gives indication on the typical level of roughness needed to allow the laminar boundary layer, i.e. $Ra, Rq = 0.1 - 1\mu m$ and $Rz < 10\mu m$.

Interestingly the presence of paint modifies the frequency of the shock unsteadiness as is illustrated in figure 14 which shows the case with paint and several cases without paint. Without paint, the frequency of the high frequency peak is lower and the influence of Mach number is conserved. The cause for this reduction in frequency is currently under investigation.

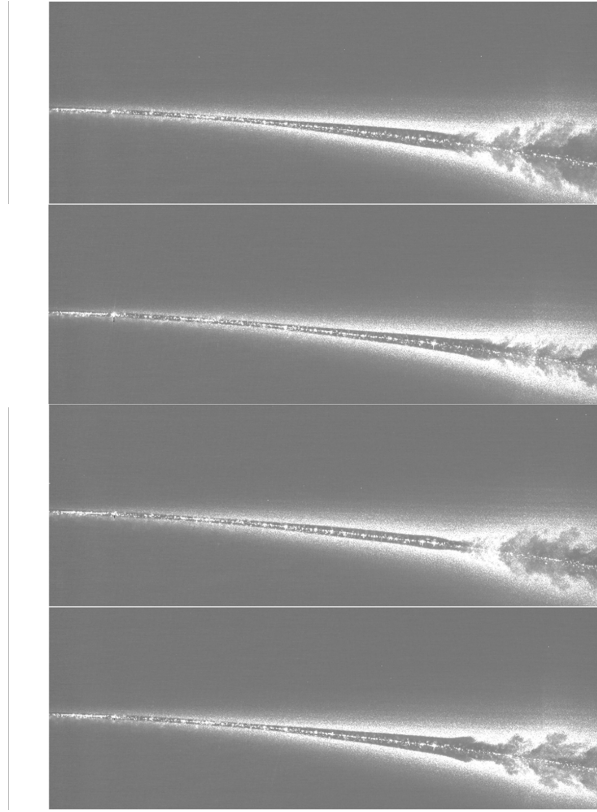


Figure 13: Laminar separation bubble visualized using PIV particles and laser lighting. The flow is for $(M, \alpha, tr) = (0.735, 4^\circ, 0)$ and exhibits the high frequency peak.

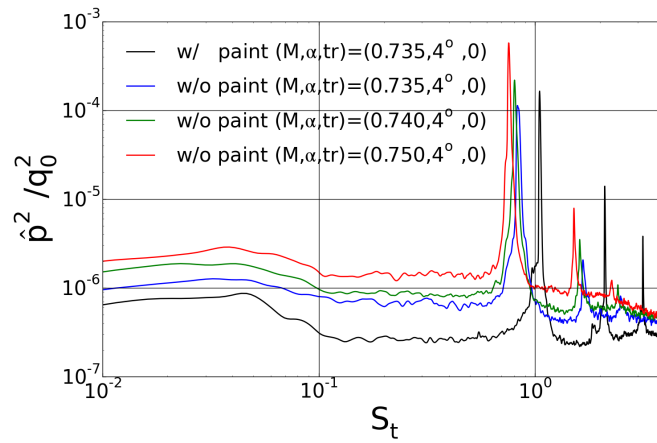


Figure 14: Influence of the paint on the pressure spectra compared to the unpainted case. The paint case comprises several Mach numbers to validate that the same Mach influence is obtained with and without paint.

Parameter	w/o paint	w/ paint (raw)	w/ paint (sandpapered)
Ra (μm)	0.3	2.4	1.6
Rq (μm)	0.4	3.1	2.0
Rz (μm)	1.75	14.7	9.0
laminar/turbulent	laminar	turbulent	laminar

Table 1: Parameters of the surface roughness with and without paint and indication of the state of the boundary layer developing on the upper surface.

4 Flow control

Two control strategies have been tested to increase the stability of the flow, three-dimensional bumps and steady jets. These devices have been developed in a separate and preliminary investigation that is not described here. The design of the bumps and jets is presented in figure 15.

The jet configuration has been designed for the test case $(M, \alpha, tr) = (0.74, 4^\circ, 0)$. The jets are located at 56.5% of chord slightly upstream of the shock wave which is at 60% of chord. Jets are oriented at pitch and toe angle of 30 and 90 degrees respectively. This inclination of the jets about the stream above the surface of the wing causes the generation of longitudinal vortices, the effect of which tends to reduce flow separation behind the shock, as was previously observed for the control of flow separation on a three-dimensional wing in the transonic regime, see Molton et al. [24]. The jet device comprises 75 jets uniformly distributed along the span, at intervals equal to $\lambda_j = 20d_j = 10mm$ where $d_j = 0.5mm$ is the jet diameter.

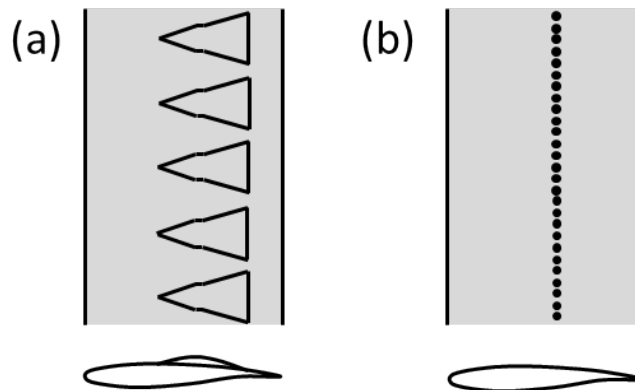


Figure 15: Schematics of the control devices. (a) three-dimensional bumps and (b) steady jets.

Bumps have been originally introduced as a method to control transonic flows in order to reduce wave drag, see Ashill et al. [6]. While wave drag at design conditions is usually minimized it strongly increases at off-design conditions when either Mach number or angle of attack is raised. This transonic drag rise can be efficiently controlled with such bumps, that contour the airfoil in order to deflect the supersonic flow at the suction side and generate oblique shock waves ahead of the main shock, which creates a more isentropic transformation. Colliss et al. [7] and Bogdansky et al. [5] showed that three-dimensional, finite-span bumps, on top of reducing wave drag, can also be advantageous to postpone buffet. The yet to be confirmed mechanism [5, 12, 6] would lie in the formation of longitudinal vorticity at the side flanks of the three-dimensional bumps, which help preventing the flow from separating behind the shock wave.

In the present setting the bump device comprises 11 bumps uniformly distributed along the span. Each bump features a wedge shape growing in width from the bump leading edge located

at 46.2% of chord to the bump trailing edge located at 80% of chord. Maximum bump height is reached at the crest at the middle of the bump and equals 0.28% of chord, i.e. 6.44mm. The crest is 10% of chord wide and 3% of chord long, and starts 17% of chord from the bump leading edge. The bump trailing edge is 21.2% of chord wide. Bumps are efficient devices for wave drag reduction and have recently been shown to enable reduction of shock wave unsteadiness.

4.1 Three-dimensional bumps

Figure 16 shows the pressure distribution about the airfoil with the bump installed compared to the baseline case. With the bumps, pressure was sampled along two separate lines, one at a spanwise location corresponding to the bump leading edge and another one in-between two bumps. It is observed that the pressure distribution is negligibly modified when bumps are present. Similarly, no difference is observed between the two spanwise locations of pressure sampling.

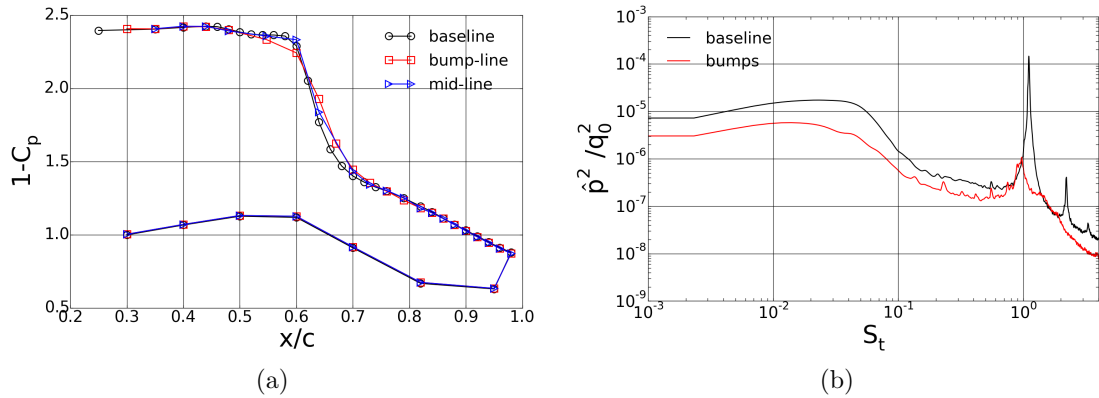


Figure 16: Effect of the bumps on (a) the pressure distribution along the airfoil and (b) pressure spectra at $x/c = 64\%$. The flow case is $(M, \alpha, tr) = (0.73, 3.5^\circ, 0)$.

Regarding flow unsteadiness, figure 16(b) shows that a reduction in intensity of the high frequency peak is achieved. Yet the flow unsteadiness remains present. This reduction of the unsteadiness seems to validate the scenario following which three-dimensional bumps generate axial vorticity which is able to limit flow separation behind the shock wave.

4.2 Steady jets

The strength of the jets is controlled using the jet momentum coefficient given by

$$C_\mu = \frac{\rho_j U_j^2 S_j}{0.5 \rho U^2 S_{ref}} \quad (1)$$

where S_{ref} is the reference surface taken here as the surface of the wing $S_{ref} = s \times c$. The value of C_μ is obtained from the total mass flow rate going through the jets, which is the parameter which is measured and controlled during the tests. Mass flow rates from 0 to 9.5g/s have been tested, which yield C_μ values from 0 to 7.5%.

Figure 17(a) shows the modification of the pressure distribution when the jets are activated. For sufficient momentum coefficient, $C_\mu > 0.065\%$, the pressure map is clearly modified and an increased lift is achieved. Looking at the pressure spectra in figure 17(b), it can be observed that the jets are able to fully stabilize the flow as the high frequency peak is suppressed from the dynamics.

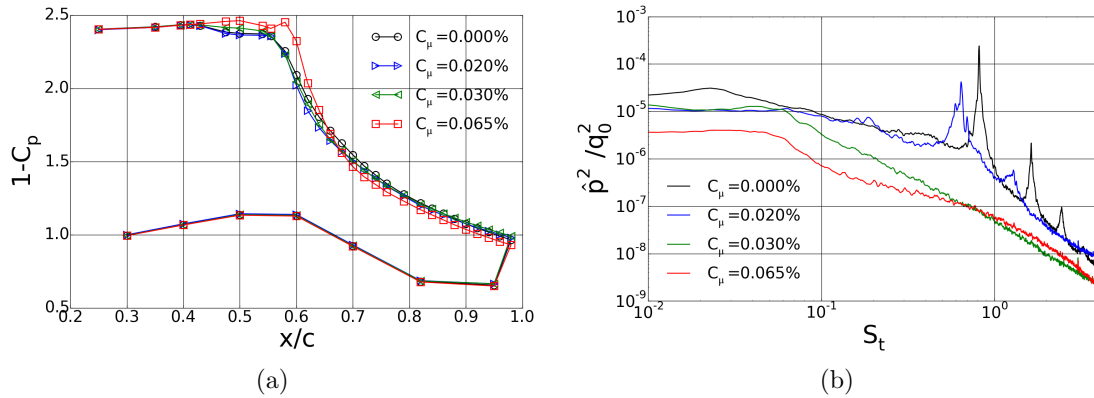


Figure 17: Effect of the jets with different C_μ values on (a) the pressure distribution along the airfoil and (b) pressure spectra. Flow case is $(M, \alpha, tr) = (0.735, 4^\circ, 0)$.

The jets were also tested in the turbulent $tr = 7$ case and the results are shown in figure 18. In the turbulent case when buffet occurs, the position of the jets is behind the mean position of the shock wave which is at about 50% of chord. Figure 18(a) shows the pressure distribution without and with control. It is observed that a significant increase in lift is achieved with the control. This is related to the suppression of the buffet phenomenon, as can be observed in figure 18(b) where the low frequency peak of the turbulent buffet phenomenon has disappeared thanks to the jet blowing.

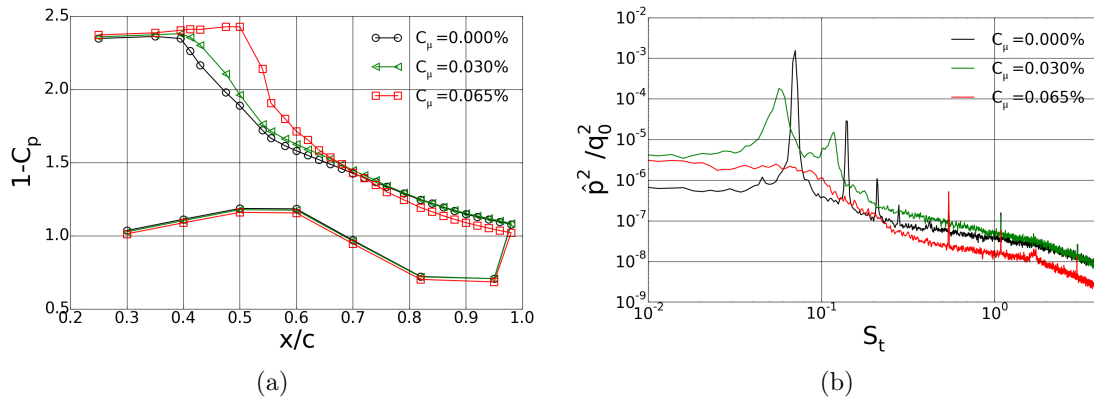


Figure 18: Effect of the jets with different C_μ values on (a) the pressure distribution along the airfoil and (b) pressure spectra. Turbulent $tr = 7$ case.

5 Conclusion

An experimental investigation of the transonic flow past a laminar wing has been accomplished in order to investigate the effect of laminarity on the stability of the flow and more particularly on the buffet phenomenon. The results reveal the existence of a critical phenomenon peculiar to the laminar case which occurs at a frequency about $S_t = 1$, in sharp contrast with the turbulent buffet phenomenon which occurs at a frequency close $S_t = 0.07$. This latter low frequency phenomenon

persists in the laminar case but with reduced amplitude and frequency, at $S_t \simeq 0.05$, and most importantly at a much less defined frequency. The shock is stronger in laminar than in turbulent. This means that the use of laminar flows to reduce drag requires to take into account all the components of drag, not only the benefit of reduced skin friction.

Flow control has been tested in order to reduce the oscillations of the flow caused by the high frequency peak, using two different control strategies, bumps and steady jet blowing. Bumps are able to partially control the flow. Jets are particularly efficient as they allow a total control of the laminar and turbulent cases.

Acknowledgements

This work has been supported by the European FP7 Project BUTERFLI (FP7-AAT-2013.8-1-RTDRUSSIA) program.

References

- [1] Holger Babinsky and John K Harvey. *Shock wave-boundary-layer interactions*, volume 32. Cambridge University Press, 2011.
- [2] G Barakos and Dimitris Drikakis. Numerical simulation of transonic buffet flows using various turbulence closures. *International Journal of Heat and Fluid Flow*, 21(5):620–626, 2000.
- [3] R. E. Bartels. Computation of shock buffet onset for conventional and supercritical airfoil. In *35th AIAA Aerospace Sciences Meeting and Exhibit*, number 97-0833, 1997.
- [4] Robert E Bartels. Flow and turbulence modeling and computation of shock buffet onset for conventional and supercritical airfoils. 1998.
- [5] Steffen Bogdanski, Klemens Nübler, Thorsten Lutz, and Ewald Krämer. Numerical investigation of the influence of shock control bumps on the buffet characteristics of a transonic airfoil. In *New Results in Numerical and Experimental Fluid Mechanics IX*, pages 23–32. Springer, 2014.
- [6] PJK Bruce and SP Colliss. Review of research into shock control bumps. *Shock Waves*, 25(5):451–471, 2015.
- [7] Simon Paul Colliss, Holger Babinsky, K Nübler, and Thorsten Lutz. Vortical structures on three-dimensional shock control bumps. *AIAA Journal*, pages 2338–2350, 2016.
- [8] Elden S Cornette. Wind-tunnel investigation of the effects of wing bodies, fences, flaps, and a fuselage addition on the wing buffet response of a transonic-transport model. 1961.
- [9] J.D. Crouch, A. Garbaruk, D. Magidov, and A. Travin. Origin of transonic buffet on aerofoils. *Journal of Fluid Mechanics*, 628:357–369, 2009.
- [10] S. Deck. Numerical simulation of transonic buffet over a supercritical airfoil. *AIAA journal*, 43(7):1556–1566, 2005.
- [11] J.B. Dor, A. Mignosi, A. Seraudie, and B. Benoit. Wind tunnel studies of natural shock wave separation instabilities for transonic airfoil tests. In *Symposium Transsonicum III*, pages 417–427. Springer, 1989.
- [12] Jeremy P Eastwood and Jerome P Jarrett. Toward designing with three-dimensional bumps for lift/drag improvement and buffet alleviation. *AIAA journal*, 50(12):2882–2898, 2012.

- [13] A Hartmann, A Feldhusen, and W Schröder. On the interaction of shock waves and sound waves in transonic buffet flow. *Physics of Fluids*, 25(2):026101, 2013.
- [14] Axel Hartmann, Michael Klaas, and Wolfgang Schröder. Time-resolved stereo piv measurements of shock–boundary layer interaction on a supercritical airfoil. *Experiments in fluids*, 52(3):591–604, 2012.
- [15] L. Jacquin, P. Molton, S. Deck, B. Maury, and D. Soulevant. Experimental study of shock oscillation over a transonic supercritical profile. *AIAA journal*, 47(9):1985–1994, 2009.
- [16] Helmut John. Critical review of methods to predict the buffet capability of aircraft. Technical report, DTIC Document, 1974.
- [17] LE Jones, RD Sandberg, and ND Sandham. Direct numerical simulations of forced and unforced separation bubbles on an airfoil at incidence. *Journal of Fluid Mechanics*, 602:175–207, 2008.
- [18] BHK Lee. Self-sustained shock oscillations on airfoils at transonic speeds. *Progress in Aerospace Sciences*, 37(2):147–196, 2001.
- [19] B.H.K. Lee and F.C. Tang. Transonic buffet of a supercritical airfoil with trailing-edge flap. *Journal of Aircraft*, 26(5):459–464, 1989.
- [20] Hans Wolfgang Liepmann. The interaction between boundary layer and shock waves in transonic flow. *Journal of the Aeronautical Sciences*, 2012.
- [21] DG Mabey. Buffeting criteria for a systematic series of wings. *Journal of Aircraft*, 26(6):576–582, 1989.
- [22] J. B. McDevitt and A. F. Okuno. *Static and dynamic pressure measurements on a NACA 0012 airfoil in the Ames high Reynolds number facility*, volume 2485. National Aeronautics and Space Administration, Scientific and Technical Information Branch, 1985.
- [23] Wolfgang Merzkirch. *Flow visualization*. Elsevier, 2012.
- [24] P Molton, J Dandois, A Lepage, V Brunet, and R Bur. Control of buffet phenomenon on a transonic swept wing. *AIAA journal*, 51(4):761–772, 2013.
- [25] Ed Obert. *Aerodynamic design of transport aircraft*. IOS press, 2009.
- [26] Edward J Ray and Robert T Taylor. Buffet and static aerodynamic characteristics of a systematic series of wings determined from a subsonic wind-tunnel study. 1970.
- [27] Theodore Alison Reyhner and I Flügge-Lotz. The interaction of a shock wave with a laminar boundary layer. *International Journal of Non-Linear Mechanics*, 3(2):173–199, 1968.
- [28] Fulvio Sartor, Clément Mettot, and Denis Sipp. Stability, receptivity, and sensitivity analyses of buffeting transonic flow over a profile. *AIAA Journal*, 53(7):1980–1993, 2014.
- [29] H. Schlichting and K. Gersten. *Boundary-layer theory*. Springer Science & Business Media, 2000.
- [30] Hermann Schlichting, Klaus Gersten, Egon Krause, Herbert Oertel, and Katherine Mayes. *Boundary-layer theory*, volume 7. Springer, 1960.
- [31] Gary S Settles. *Schlieren and shadowgraph techniques: visualizing phenomena in transparent media*. Springer Science & Business Media, 2012.

- [32] Q. Xiao, H. Tsai, and F. Liu. Numerical study of transonic buffet on a supercritical airfoil. *AIAA journal*, 44(3):620–628, 2006.